Nanoplasmonic triple-wavelength demultiplexers in two-dimensional metallic waveguides

H. Lu · X.M. Liu · L.R. Wang · D. Mao · Y.K. Gong

Abstract A novel kind of plasmonic wavelength demultiplexers (WDMs) based on two-dimensional metal–insulator–metal waveguides with side coupled nanocavities (SC-NCs) is proposed and numerically investigated. The WDMs contain three waveguide output channels, each of which functions as a dual-stopband plasmonic filter. The demultiplexing wavelengths can be tuned by controlling the lengths and widths of SCNCs. The finite-difference time-domain results can be accurately analyzed by the resonant theory of nanocavity. Our structures have important potential applications for design of WDM systems in highly integrated optical circuits.

1 Introduction

Electromagnetic waves trapped on metal-dielectric interfaces and coupled to propagating free electron oscillations in the metals, known as surface plasmon polaritons (SPPs), are considered as the most potential way for realization of highly integrated optical circuits due to significant overcoming of classical diffraction and manipulation of light in a nanoscale domain [1–3]. A number of devices based on SPPs, such as Mach–Zehnder interferometers [2, 4], all-optical switches [5], splitters [2, 6], modulators [7], beam manipulator [8, 9], multiplexing sensor [10], polarization analyzer [11], optical amplifier [12], optical buffers [13], Bragg reflectors [14, 15], mirrors [16], and waveguides [17,

18] have been simulated numerically and demonstrated experimentally. With the development of artificial fabrication, these devices may be fabricated and applied in future integrated optical circuits. The conventional wavelength demultiplexers (WDMs) in modern optical devices and communications perform excellent wavelength-filtering function [19]. But these WDMs have large dimension and could not be utilized in highly integrated optical circuits due to the diffraction limit. Among the plasmonic devices, waveguides consisted of metal–dielectric–metal (MIM) structure have strong confinement of light in the insulator region with an acceptable length for SPP propagation [15]. MIM plasmonic waveguides are promising for the design of nanoscale all-optical devices owing to a relatively easy fabrication according to the current state of the art [20, 21]. Recently, the two-dimensional (2D) SPP devices on the basis of MIM waveguides have been reported theoretically [4, 8, 22–30] and experimentally [2, 3, 17, 18, 20]. To utilize SPPs at the information technology level, some simple wavelength-selective structures based on 2D MIM waveguides have been proposed, such as tooth-shaped filters [22], plasmonic filters with ring, rectangular, and disk-shaped resonators [23–27]. As key factors in these structures, optical resonators will be principal constituent elements of future plasmonic wavelength-selective devices due to their simplicity, symmetry, and ease of fabrication [28]. Plasmonic wavelength demultiplexers (WDMs) will play very important role in the future all-optical communication systems [29]. Noual et al. designed a plasmonic two-wavelength demultiplexer based on Y-bent MIM plasmonic waveguides with two rejective or selective filters in two branches [30]. The device needs a distance of at least 1.5 μm between the cavities inside the Y waveguide and the input port. A plasmonic demultiplexer structure based on metallic grating in three-dimensional (3D) free space has been reported [31]. The

H. Lu · X.M. Liu (✉) · L.R. Wang · D. Mao · Y.K. Gong
State Key Laboratory of Transient Optics and Photonics, Xi'an
Institute of Optics and Precision Mechanics, Chinese Academy
of Sciences, Xi'an 710119, China
e-mail: liuxueming72@yahoo.com
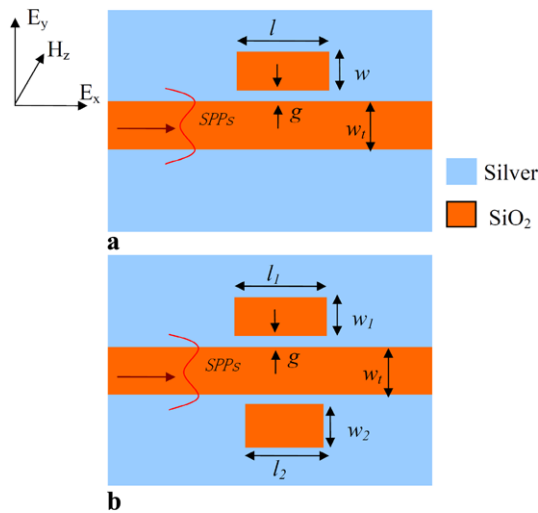Fax: +86-29-88887603

Fig. 1 Schematic diagrams of MIM waveguides with (**a**) single SCNC, (**b**) two SCNCs

dimension of this structure would exceed wavelength scale due to the array of periodic elements and 3D conformation.

In this paper, we propose and numerically investigate a new kind of nanoscale plasmonic triple-wavelength demultiplexers based on 2D MIM waveguide with dual-stopband plasmonic filters in three output branches by the finite-difference time-domain (FDTD) method. The demultiplexing wavelengths are easily tunable by controlling the lengths and widths of side coupled nanocavities (SCNCs), which can be accurately analyzed by the resonant theory of rectangular nanocavity. By selecting appropriate geometric parameters, a demultiplexing structure of three wavelengths is designed to investigate the characteristics of SPP propagation. Our compact structures have extensive potential for design of WDM systems and realization of optical computing in highly integrated optical circuits.

2 Principle of dual-stopband plasmonic filters

The MIM plasmonic waveguide consists of two metallic claddings and a dielectric core with the width w_t, as shown in Fig. 1. There exist two types of plasmonic modes in MIM waveguides, i.e., the antisymmetric mode and the symmetric mode. The symmetric mode exhibits cut-off when w_t goes below a cut-off width which is about hundreds of nanometers [14]. Since w_t in our configuration is below the cut-off width, the antisymmetric mode is only taken into account. When TM-polarized plane light wave is injected to the MIM structure, the incident light will be coupled into the waveguide and the SPP waves are formed on the two metal interfaces. As shown in Fig. 1(a), when a rectangular nanocavity is built on the side of the MIM waveguide, the incident power is partly coupled into the cavity. Stable standing waves can build up constructively in the cavity when the

resonant condition is satisfied. Based on the resonant theory of rectangular cavity [24], the resonance wavelength can be given by

$$\lambda_m = \frac{2\mathrm{Re}(n_\mathrm{eff})l}{m - (\varphi_\mathrm{ref1} + \varphi_\mathrm{ref2})/2\pi}, \tag{1}$$

where ϕ_ref1 and ϕ_ref2 represent the reflective phase shifts on the left and right sides of the nanocavity, respectively. l is the length of cavity and n_eff is the effective refractive index of SPPs in the cavity. m is a integer and stands for the m-th order resonant mode. From (1), it is found that the resonance wavelengths are proportional to l. Meanwhile, the resonance wavelengths are related with n_eff. Here, n_eff is related with the incident wavelength λ and the width w of SCNC. Their relation is as follows [14, 32, 33]:

$$\varepsilon_m k_d \tanh\left(\frac{w k_d}{2}\right) + \varepsilon_d k_m = 0, \tag{2}$$

$$k_{d,m} = \sqrt{\beta_\mathrm{spp}^2 - \varepsilon_{d,m} k_0^2}, \tag{3}$$

$$n_\mathrm{eff} = \beta_\mathrm{spp}/k_0, \tag{4}$$

where ε_d and ε_m are the dielectric constant of SCNC and metal cladding. k_d and k_m are transverse propagation constants of the dielectric and metal, respectively. β_spp represents the complex propagation constant of SPP waves. $k_0 = 2\pi/\lambda$ is the wavevector of incident light in vacuum. In the MIM waveguide, the metal is assumed as silver, whose frequency-dependent complex relative permittivity can be described by the well-known Drude model [22]

$$\varepsilon_m(w) = \varepsilon_\infty - \frac{w_p^2}{w(w + i\gamma)}, \tag{5}$$

where ε_∞ is the dielectric constant at the infinite frequency, γ and ω_p represent the electron collision frequency and bulk plasma frequency, respectively. ω is the angular frequency of incident light. The parameters for silver can be set as $\varepsilon_\infty = 3.7$, $\omega_p = 9.1$ eV, and $\gamma = 0.018$ eV. These parameters describe the angular frequency dependency of silver with best fit for the free-space wavelength from 400 to 2000 nm [14]. The insulator is set as SiO₂ ($n_d = 1.46$). n_eff can be obtained by solving (2)–(5). The real part of n_eff (i.e., $\mathrm{Re}(n_\mathrm{eff})$) as a function of w at different wavelengths is obtained and shown in Fig. 2.

As aforementioned, the power coupling from the waveguide into SCNC will give rise to the excitation of resonant mode when the resonant condition is satisfied [30, 33]. Simultaneously, the power in SCNC partly escapes into the waveguide, and generates a series of interference with the SPP waves in the waveguide. Thus, the transmission spectrum exhibits a dip at the resonance wavelength. The structure is regarded as a rejection (or stop-band) plasmonic fil-
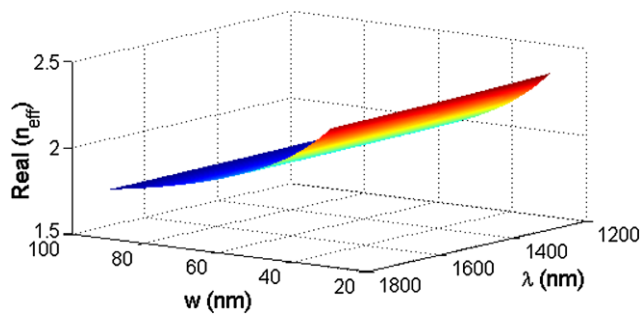
Fig. 2 Real part of n_{eff} versus the incident wavelength λ and width w of SNCN
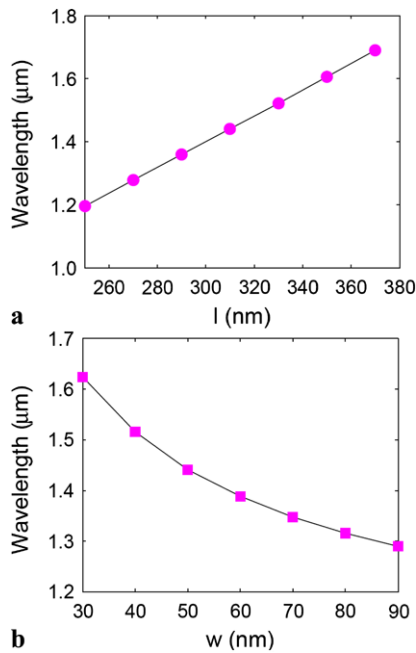

Fig. 3 Transmitted-dip wavelengths versus (**a**) the length l of SCNC with $w = 50$ nm, (**b**) the width w of SCNC with $l = 310$ nm

ter. Here, the relationship between the two geometric parameters (i.e., l and w in Fig. 1(a)) and the transmitted-dip wavelength is investigated by FDTD simulations. In the FDTD algorithm, the spatial steps are set as $\Delta x = 5$ nm and $\Delta y = 5$ nm [4, 24, 32], which are sufficient for the convergence of numerical results. The temporal step is $\Delta t = \Delta x/2c$. The metal slit width w_t and gap width g are respectively set as 50 and 15 nm, which are similar to that of other MIM waveguides [22, 33]. The geometrical parameters in our simulations are ideal and the introduced roughness in reality is neglected. Figure 3(a) reveals that the transmitted-dip wavelength has a linear relationship with l of SCNC. Figure 3(b) shows that there exists a nonlinear relationship between the transmitted-dip wavelength and the width w of SCNC. The results can be explained by the dispersion relation and resonant theory of rectangular nanocavity. As can be seen in Fig. 2, $\mathrm{Re}(n_{eff})$ performs invariable for wave-
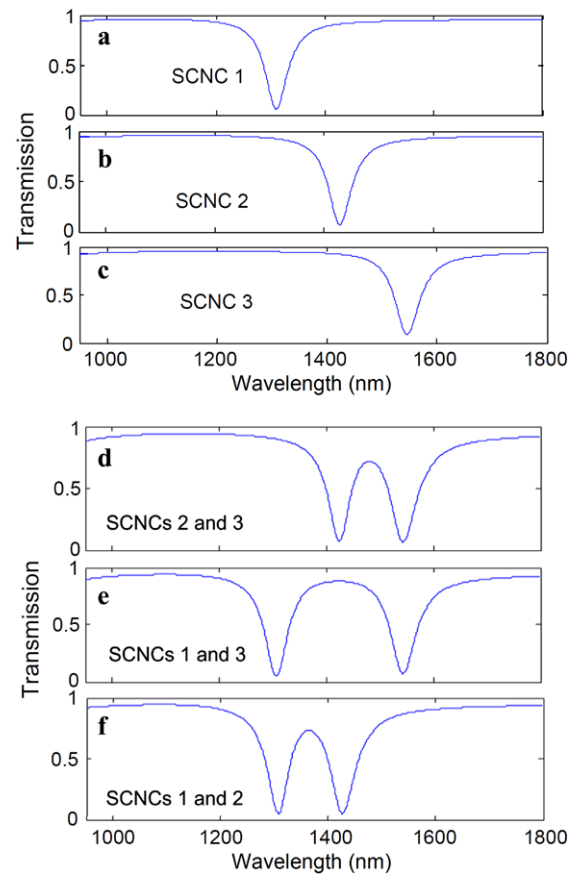

Fig. 4 Transmission spectra with a dip at the wavelength of (**a**) 1310 nm, (**b**) 1425 nm, and (**c**) 1550 nm. Transmission spectra with two dips at the wavelengths of (**d**) 1425 and 1550 nm, (**e**) 1310 and 1550 nm, (**f**) 1310 and 1425 nm

lengths in the range of 1200–1800 nm. From (1), the resonance wavelength is in proportion to the length of SCNC with fixed $\mathrm{Re}(n_{eff})$. $\mathrm{Re}(n_{eff})$ exhibits a nonlinear decrease with the increase of w at arbitrary wavelengths from 1200 to 1800 nm, as shown in Fig. 2. Thus, the resonance wavelength nonlinearly decreases for increasing w with fixed l. Therefore, the transmitted-dip wavelength of the stop-band plasmonic filter can be tuned by controlling the length and width of SCNC. By choosing appropriate geometrical parameters of the structure, three stop-band plasmonic filters with the transmitted-dip wavelengths of 1310, 1425, and 1550 nm are obtained and their transmission spectra are shown in Figs. 4(a)–(c). A 2-tuple (l, w) is utilized to describe the parameters of SCNC. The above chosen geometrical parameters of SCNC are ($l = 285$ nm, $w = 60$ nm), ($l = 315$ nm, $w = 60$ nm), and ($l = 350$ nm, $w = 60$ nm). We name these cavities as SCNC "1", "2", and "3", respectively. As can be seen in Fig. 1(b), two SCNCs are placed on the sides of the MIM waveguide to investigate the transmission properties. Three transmission spectra are obtained by two-two combination of the above three SCNCs. As shown in Figs. 4(d)–(f), the transmission spectra exhibit two dips
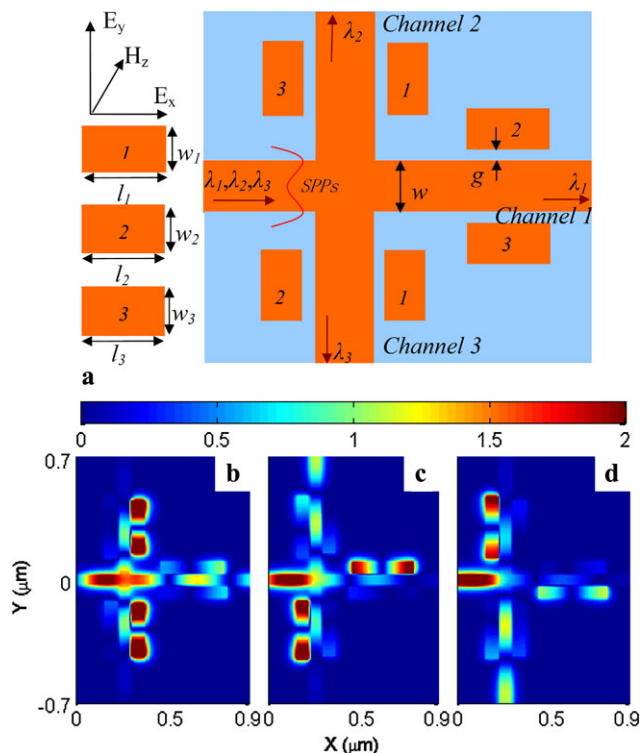
Fig. 5 (**a**) Schematic diagram of our WDM. (**b**)–(**d**) Field distributions of $|H_z|$ with incident wavelengths of 1310, 1425, and 1550 nm

4 Conclusions

In this paper, we have proposed and numerically investigated a novel kind of triple-wavelength demultiplexers based on 2D MIM waveguides with dual-stopband plasmonic filters in three output branches. By FDTD simulations, we find that the demultiplexing wavelengths λ_1, λ_2, and λ_3 can be tuned in the near infrared range by controlling the lengths and widths of SCNCs 1, 2, and 3, respectively. The results can be accurately analyzed by the resonant theory of rectangular nanocavity. By selecting appropriate geometric parameters, a WDM with three wavelengths (i.e., 1310, 1425, and 1550 nm) has been designed to investigate the characteristics of SPP propagation. Important future practical applications of plasmonic structures are strongly dependent on further theoretical advances [3]. Therefore, our design, simulation, and analysis are meaningful and helpful for the fabrications and further researches of SPP WDMs in high-integration optical communications and computing.

which indicate dual-stopband plasmonic filters. Meanwhile, it is found that the transmitted-dip wavelengths are consistent with that of stop-band filters with single SCNC. Thus, we can easily tune the transmitted-dip wavelengths of dual-stopband plasmonic filters by selecting proper geometric parameters, such as the lengths and widths of SCNCs.

3 Triple-wavelength demultiplexer

The above dual-stopband plasmonic filters are utilized to design a triple-wavelength demultiplexer. As shown in Fig. 5(a), the WDM has three output channels, each of which consists of a MIM waveguide and two SCNCs. Three demultiplexing wavelengths are $\lambda_1 = 1310$ nm, $\lambda_2 = 1425$ nm, and $\lambda_3 = 1550$ nm. Figures 5(b)–(d) depict the field distributions of $|H_z|$ with incident wavelengths of 1310, 1425, and 1550 nm, respectively. It is found that the incident lights with the wavelengths of 1310, 1425, and 1550 nm, respectively, excite resonant modes in SCNCs 1, 2, and 3, as well as are reflected in corresponding waveguides. Thus, channels 1, 2, and 3 only permit light propagation at wavelength of 1310, 1425, and 1550 nm, respectively. The results are in good agreement with the transmission spectra in Figs. 4(d)–(f). According to the discussion in Sect. 2, the geometric parameters such as lengths and widths of SCNCs on the side of waveguides can manipulate the demultiplexing wavelengths.

References

1. W.L. Barnes, A. Dereux, T.W. Ebbesen, Nature **424**, 824 (2003)
2. S.I. Bozhevolnyi, V.S. Volkov, E. Devaux, J.Y. Laluet, T.W. Ebbesen, Nature **440**, 508 (2006)
3. D. Gramotnev, S. Bozhevolnyi, Nat. Photonics **4**, 83 (2010)
4. B. Wang, G.P. Wang, Opt. Lett. **29**, 1992 (2004)
5. G.A. Wurtz, R. Pollard, A.V. Zayats, Phys. Rev. Lett. **97**, 057402 (2006)
6. A. Evlyukhin, S. Bozhevolnyi, A. Stepanov, J. Krenn, Appl. Phys. B **84**, 29 (2006)
7. T. Nikolajsen, K. Leosson, S.I. Bozhevolnyi, Appl. Phys. Lett. **85**, 5833 (2004)
8. C. Min, P. Wang, X. Jiao, Y. Deng, H. Ming, Appl. Phys. B **90**, 97 (2008)
9. L.L. Yin, V.K. Vlasko-Vlasov, J. Pearson, J.M. Hiller, J. Hua, U. Welp, D.E. Brown, C.W. Kimball, Nano Lett. **5**, 1399 (2005)
10. D.V. Oosten, M. Spasenovic, L. Kuipers, Nano Lett. **10**, 286 (2010)
11. S.Y. Yang, W.B. Chen, R.L. Nelson, Q.W. Zhan, Opt. Lett. **34**, 3047 (2009)
12. I.D. Leon, P. Berini, Nat. Photonics **10**, 1 (2010)
13. Q.Q. Gan, Y.J. Ding, F.J. Bartoli, Phys. Rev. Lett. **102**, 056801 (2009)
14. J. Park, H. Kim, B. Lee, Opt. Express **16**, 413 (2008)
15. B. Wang, G.P. Wang, Appl. Phys. Lett. **87**, 013107 (2005)
16. S. Randhawa, M.U. González, J. Renger, S. Enoch, R. Quidant, Opt. Express **18**, 14496 (2010)
17. S.I. Bozhevolnyi, V.S. Volkov, E. Devaux, T.W. Ebbesen, Phys. Rev. Lett. **95**, 046802 (2005)
18. B. Lamprecht, J.R. Krenn, G. Schider, H. Ditlbacher, M. Salerno, N. Felidj, A. Leitner, F.R. Aussenegg, Appl. Phys. Lett. **79**, 51 (2001)
19. L. Poladian, Opt. Lett. **26**, 7 (2001)

20. P. Neutens, P. Van Dorpe, I. De Vlaminck, L. Lagae, G. Borghs, Nat. Photonics **3**, 283 (2009)
21. J.A. Dionne, L.A. Sweatlock, H.A. Atwater, A. Polman, Phys. Rev. B **73**, 035407 (2006)
22. X.S. Lin, X.G. Huang, Opt. Lett. **33**, 2874 (2008)
23. A. Hosseini, Y. Massoud, Appl. Phys. Lett. **90**, 181102 (2007)
24. Q. Zhang, X.G. Huang, X.S. Lin, J. Tao, X.P. Jin, Opt. Express **17**, 7549 (2009)
25. A. Noual, Y. Pennec, A. Akjouj, B. Djafari-Rouhani, L. Dobrzynski, J. Phys., Condens. Matter **21**, 375301 (2009)
26. H. Lu, X.M. Liu, D. Mao, L.R. Wang, Y.K. Gong, Opt. Express **18**, 17922 (2010)
27. G. Wang, H. Lu, X. Liu, D. Mao, L. Duan, Opt. Express **19**, 3513 (2011)
28. I. Chremmos, J. Opt. Soc. Am. A **26**, 2623 (2009)
29. A. Drezet, D. Koller, A. Hohenau, A. Leitner, F.R. Aussenegg, J.R. Krenn, Nano Lett. **7**, 1697 (2007)
30. A. Noual, A. Akjouj, Y. Pennec, J.N. Gillet, B. Djafari-Rouhani, New J. Phys. **11**, 103020 (2009)
31. M.S. Kumar, X. Piao, S. Koo, S. Yu, N. Park, Opt. Express **18**, 8800 (2010)
32. Y. Gong, L. Wang, X. Hu, X. Li, X. Liu, Opt. Express **17**, 13727 (2009)
33. Z. Zhong, Y. Xu, S. Lan, Q. Dai, L. Wu, Opt. Express **18**, 79 (2010)